Heliyon

ELSEVIER

Received:
14 June 2018
Revised:
21 September 2018
Accepted:
5 November 2018

Cite as: Govinda Mahajan, Scott M. Thompson, Heejin Cho. Experimental characterization of an n-pentane oscillating heat pipe for waste heat recovery in ventilation systems. Heliyon 4 (2018) e00922. doi: 10.1016/j.heliyon.2018.e00922

Experimental characterization of an n-pentane oscillating heat pipe for waste heat recovery in ventilation systems

Govinda Mahajan [a], **Scott M. Thompson** [b], **Heejin Cho** [c,*]

[a] *Rheem Manufacturing, 2600 Gunter Park Dr., Montgomery, AL, 36109, USA*

[b] *Department of Mechanical Engineering, Auburn University, Wiggins Hall, 354 War Eagle Way, Auburn, AL, 36849, USA*

[c] *Department of Mechanical Engineering, Mississippi State University, 210 Carpenter Engineering Building, P.O. Box 9552, Mississippi State, MS, 39762, USA*

[*] Corresponding author.

E-mail address: cho@me.msstate.edu (H. Cho).

Abstract

A tubular oscillating heat pipe (OHP), with long form factor and 1 × 0.5 m^2 footprint, was experimentally characterized for passive waste heat recovery via air-to-air heat exchange in a typical Heating Ventilation & Air Conditioning (HVAC) ducting system. Experiments were designed to demonstrate the OHP's ability to utilize otherwise wasted thermal energy to pre-heat or pre-cool air for reducing building energy consumption. Results indicate that the OHP is fully-capable of operating while possessing a relatively long form factor (>1 m) and as a forced convection, air-to-air heat exchanger for waste heat recovery in HVAC systems.

Keywords: Energy, Mechanical engineering

1. Introduction

The energy invested for operating heating, ventilation and air conditioning (HVAC) systems accounts for approximately 60% of the world's total building energy

https://doi.org/10.1016/j.heliyon.2018.e00922

consumption [1], and this portion will rise along with population growth and levels of prosperity [2]. The generation and implementation of cost-effective technologies that improve HVAC efficiency, including unique waste heat recovery methods, continues to be sought. In fact, a study reported to the U.S. Department of Energy [3] indicates that through the use of currently available energy recovery/management technologies, it is possible to reduce a building's energy consumption by up to 50%. The study also indicated that advanced waste heat recovery/ventilation technologies can significantly reduce the energy needed to condition ventilation make-up air by utilizing the often neglected temperature potential between cold/hot air streams in HVAC duct systems. This temperature potential can drive heat transfer through, for example, air-to-air heat exchangers; thus allowing for air pre-cooling and/or pre-heating for reducing power demand on air conditioning (AC) and heating units.

Examples of waste heat recovery/ventilation technology include: flat plate heat exchangers, enthalpy (or energy) wheels, heat pipe heat exchangers and oscillating heat pipe heat exchangers (OHP-HEs). The typical effectiveness for flat plate heat exchangers and enthalpy wheels range between 50-70% and 50−85%, respectively; while pressure drops are 24−374 Pa and 100−175 Pa, respectively [4]. In general, flat plate heat exchangers tend to have a lower effectiveness as compared to enthalpy wheels; however, they often cost less (i.e., ~$1.0/CFM for flat plate heat exchangers and ~1.5/CFM for wheels) and require less maintenance than enthalpy wheels since they consist of no moving parts [3].

A heat pipe heat exchanger [5] typically consists of a bundle/array of conventional heat pipes arranged for optimized heat transfer and pressure drop. The conventional heat pipe is a proven two-phase heat transfer device that consists of a thermally-conductive, metallic shell (i.e. pipe) with an internal wicking structure, such as sintered mesh screens or particles and/or co-axial grooves, and a working fluid [6]. One end of the device is located near a heat source, forming its evaporator − where the encapsulated fluid evaporates, while the other end is located near a heat sink, forming its condenser − where fluid condenses. This evaporation/condensation cycle allows the conventional heat pipe to have an ultra-high heat transport capability; justifying its broad application in the electronics and aerospace industries for the past half century [7]. However, the conventional heat pipe has operating limitations that restrict and challenge its design, such as the entrainment, sonic and boiling limitations [6]. Since a wicking structure is often required for their efficient performance, conventional heat pipes are relatively difficult to manufacture.

The oscillating heat pipe (OHP), another passive-type, two-phase heat transfer device, exists as a closed-loop, serpentine-arranged capillary tube partially filled with a suitable liquid [8]. Since the internal diameter of the OHP tube is at the capillary scale, a natural liquid-vapor/slug-plug system can be formed upon working fluid introduction [9]. The serpentine-arranged tube meanders to and through a hot and

https://doi.org/10.1016/j.heliyon.2018.e00922

cold section repeatedly; forming its evaporator and condenser, respectively. As shown in Fig. 1, this results in the evaporator and condenser having 'U-sections', also known as 'turns'. Heating and cooling the turns of the OHP results in phase change of the encapsulated liquid and the production of thermally unstable vapor plugs in the evaporator. Due to combative vapor pressures in adjacent tube sections, an oscillatory, two-phase flow field is created. Thermal energy is efficiently transported in the OHP via the oscillatory motion of liquid slugs and vapor plugs due to both sensible and latent heat transfer. Similar to the conventional heat pipe, the OHP needs a minimum heat input (or temperature difference) to initiate fluid motion [10, 11]; once attained, it can achieve very high effective thermal conductivities on-the-order of 10,000 W/m-K [12].

Many experimental studies have been carried out to characterize the thermal performance of the OHP, and it is now well accepted that its performance is sensitive to its design, working fluid selection [13, 14, 15], frequency of oscillation [16], volume fill ratio, internal flow pattern [9, 17], operating temperature [18], OHP aspect ratio [19], operating orientation, and more [20]. In addition, several analytical models have been proposed to predict the OHP thermal performance [15, 21, 22]. Unique design features have also been investigated for improving OHP performance; including the installation of floating ball check valves [14, 23]. Utilization of check valves within an OHP can result in rectification of the highly oscillatory fluid motion and thus promote a common flow direction through the evaporator for increased heat transfer.

Unlike the conventional heat pipe, the OHP requires no internal wicking structure to operate [9] and has fewer operating limitations [24]. Moreover, the vapor and liquid motion in the OHP is segregated, hence the liquid flow is not altered by the vapor flow [25]. Due to its passive operation, ability to operate in many orientations [26], and ease of construction [19], the OHP has become an attractive heat transfer device in the last two decades for a variety of applications [20].

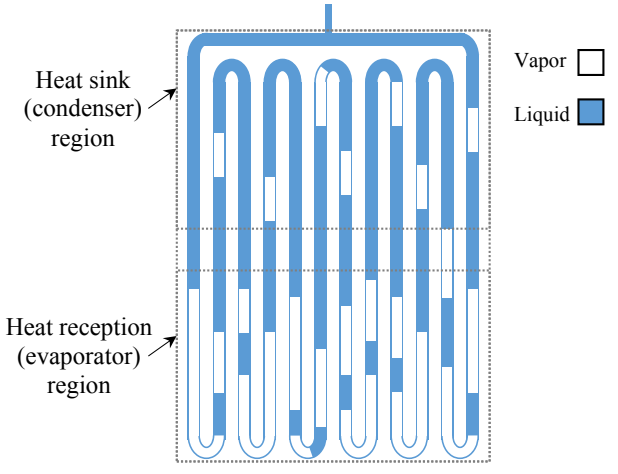

Fig. 1. Two-phase fluid (vapor and liquid) distribution within a tubular OHP.

https://doi.org/10.1016/j.heliyon.2018.e00922

The majority of experimental work conducted on the OHP has employed constant heat flux or constant-temperature evaporator conditions for simulating electronics-cooling applications [5, 20]. However, only limited studies have focused on characterizing the OHP for its use in HVAC or energy-related systems. The heating/cooling configurations encountered in these types of systems involve forced convection with air on either side; with the number and location of air streams varying based on HVAC application. Supirattanakul et al. [23] investigated the thermal performance of a copper tube OHP integrated in single stream, split type AC system. The OHP, which was filled with various refrigerants, consisted of 56 turns and floating ball check valves were integrated for flow control. The device consisted of a 'two flow plane' design with its evaporator (220 mm long) in front of the AC cooling coil (for air preheating) and its condenser (220 mm long) downstream, behind the AC cooling coil (for air reheating). The OHP was found to increase the coefficient of performance (COP) of a split type AC system by 14.9%.

Khandekar and Gupta [27] embedded a 150 mm long tubular OHP into various flat, metallic plates for enhancing space radiator systems. It was found that it is only advantageous to embed OHPs for enhanced thermal spreading and subsequent plate radiation for conditions in which plate material possesses low thermal conductivity. Rittidech et al. [28] utilized multiple open-looped, tubular OHPs for preheating air by positing the OHP evaporator in the exhaust stream of a batch-type dryer with burner. The OHPs, filled with R123 or water, consisted of 8 turns and an evaporator and condenser with 19 cm length each. A total of 32 OHPs were bundled into an array for 50 °C exhaust gas heat recovery. Results demonstrated that a maximum OHP bundle effectiveness of 0.54 could be achieved when using R123 as the working fluid. Meena et al. [14] also demonstrated the utility of OHPs for air preheating via OHP integration to the air drying cycle. Closed-loop, copper OHPs (2 mm inner diameter) with floating ball check valves were used, providing a footprint of 0.4 m^2. It was reported that, for an air flow velocity of 0.5 m/s, the heat transfer effectiveness of OHP preheater increased from 0.39 to 0.47 when the temperature of the hot air stream increased from 50 to 70 °C. Dilawar et al. [29] numerically studied the oscillatory behavior of single turn OHP filled with n-pentane, ethanol, and water. The study predicted that oscillation with n-pentane would be characterized by low frequency and high amplitude. In comparison to water and ethanol, it would require less vapor pressure differential to attain start-up heat flux. Burban et al. [30] developed a 16 turn copper/un-looped OHP intended for electronic thermal management in a hybrid vehicle. The OHP was tested with four different working liquids – n-pentane, methanol, water, and acetone. The study found that among all working liquids investigated; n-pentane works best in low temperature and low airflow environments.

The current work focuses on characterizing the utility of a single closed-loop, tubular OHP for enhancing the efficiency of ducted AC systems (or space heating systems)

https://doi.org/10.1016/j.heliyon.2018.e00922

via waste heat recovery and air-to-air heat exchange. A unique, large form factor OHP is fabricated and shown to effectively operate, within a forced-convection environment typical to adjacent-duct HVAC systems. A novel, environmentally-friendly working fluid with properties unique for low-grade heat flux conditions, i.e. n-pentane, has been investigated for characterizing the OHP's adaptability to waste heat recovery applications. The OHP thermal resistance and other heat transfer characteristics were compared to an empty/evacuated OHP with same overall dimensions. The OHP aerodynamic performance, in terms of pressure drop, was evaluated and juxtaposed with the heat transfer characteristics.

2. Design

A copper capillary tube (inner diameter $D_i = 0.165$ cm and outer diameter $D_o = 0.317$ cm) was used for constructing a 9-turn OHP-HE with tube-sections separated by a distance of 22 mm (nominal). In order to segregate the liquid and vapor volumes inside the OHP via capillary action, the inner tube radius, r_i, was ensured to satisfy Eq. (1). As shown in Eq. (1), the critical Bond number (Bo_c), local gravity conditions (g), working fluid density (ρ), as well as working fluid surface tension (σ), dictate capillary action [31]. The critical Bond number has been found to range between 0.8 - 1.0 [32].

$$r_i \lesssim Bo_c \sqrt{\frac{\sigma}{g(\rho_l - \rho_v)}} \tag{1}$$

The OHP was designed to possess a footprint of 60 × 45 cm^2; to enable its direct integration within typical-sized air ducts found in many commercial buildings, i.e. ~63 × 51 cm^2. Fig. 2 provides a schematic of the conceived OHP-to-duct integration and a photograph of the copper OHP investigated in this study.

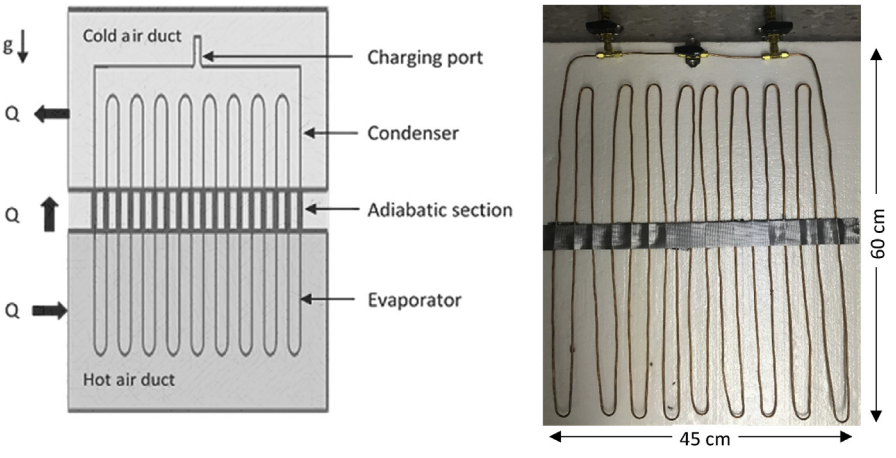

Fig. 2. Schematic of the OHP-HE position relative to hot and cold air ducts (left) and a photograph of the OHP-HE investigated (right).

https://doi.org/10.1016/j.heliyon.2018.e00922

The OHP was first evacuated of air using a dual−seal vacuum pump (Welch Scientific Co., Model 1400) to an approximate vacuum pressure of 6.67 (±0.667) Pa (50 ± 5 mTorr). After evacuation, the OHP was filled with n-pentane (99%, reagent grade, ACS) at a liquid-to-OHP volume ratio (fill ratio) of either 0 (+2) % (i.e., empty), 60 (±2) % or 70 (±2) %. Pentane was selected for its relatively low boiling point, low dynamic viscosity and latent heat of evaporation. In addition, n-pentane is non-toxic [33] and non-ozone-depleting [34] making it a feasible candidate for HVAC application.

3. Experimental

The OHP was experimentally characterized for air-to-air heat exchange in a typical HVAC system with adjacent, unmixed air streams at different temperatures representative of winter-time operating conditions. As shown in Fig. 3, the hot and cold air streams were generated and constrained within two cross-flow wind tunnels equipped with air heaters (Brasch Electroduct AG2002-001075 and TUTCO Heat Pack/81-0578-00) with combined heating capacity of 5 (±0.05) kW. Both air ducts were equipped with two centrifugal fan units (Continental/AXC150B-ES) located upstream and downstream from the OHP. Each air duct consisted of 15.24 cm diameter circular aluminum ducts attached with custom-made diffusers/nozzles to provide for HVAC-typical exit plane dimensions of 45.72 cm × 60.96 cm. An operating environment typical of a US Southeast winter was simulated for this proof-of-concept experiment. The cold air stream was taken at an ambient temperature of 6 (±1) ^{o}C in the topmost wind tunnel and the hot air stream was taken at a room temperature of 11 (±1) ^{o}C and heated to 45 (±1) ^{o}C within the bottom wind tunnel. This air stream configuration allowed the OHP to be in the preferred vertical-bottom heating orientation for optimal performance. Both air streams had a volumetric flow rate of 0.19 (±0.01) m^3/s. Fiber blanket insulation (R-19) was added around the ducts and diffuser/nozzle to reduce inter-stream heat exchange. Total heat loss from the

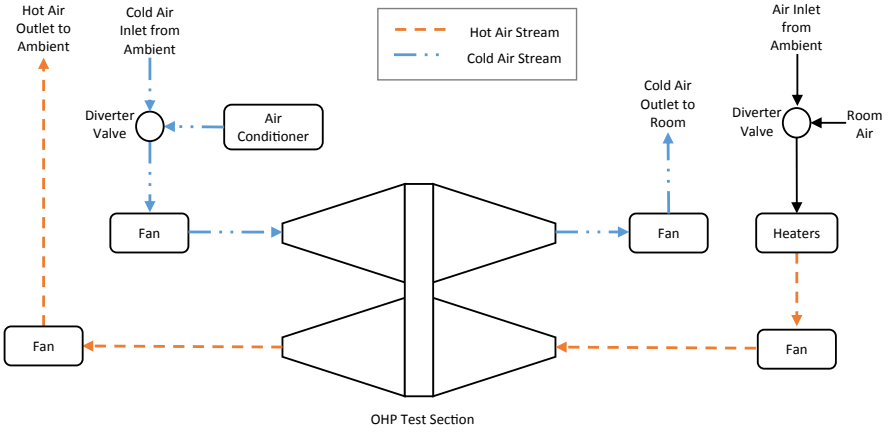

Fig. 3. Schematic diagram of OHP-HE experimental setup.

https://doi.org/10.1016/j.heliyon.2018.e00922

hot stream during experimentation was estimated to be approximately 5% that of OHP heat transfer. Fig. 3 provides a schematic of the apparatus and essential components used for the experimental investigation.

Six type-T thermocouples (Omega) were used to measure the temperature along the OHP surface, three of which were taped on the center-most tubes along the OHP evaporator and three similarly positioned on the OHP condenser. Additional type-T thermocouples were routed in with a small tube in the air duct and placed deep near to center of the duct to measure the temperature of the air streams. Pressure sensors (Omega/PX653−0.255V) were used to measure pressure differential and flow rates within the two air streams. These sensors were placed in the middle of the air streams and were connected to a data acquisition (DAQ) system (National Instruments TC-2095/SCXI-1100). Fig. 4 shows the approximate locations of the thermocouples and pressure sensors. Table 1 summarizes the physical characteristics of the OHP and experimental apparatus.

A portable calibrator (Omega/CL3515R) was used to calibrate all thermocouples and the DAQ system; an offset, if found, was added for data correction. Air prevailing inside the wind tunnel was forced to exit the system by starting the air circulation 15 minutes prior to start of experiments. SignalExpress 2013 (National Instruments) DAQ software was used to record measurements during experimentation. Temperature measurements were recorded at a frequency of 10 Hz. During OHP testing, sufficient time was given to allow OHP temperature oscillations to achieve a steady mean temperature. The OHP was tested with either 60% or 70% by-volume n-pentane fill ratios or while empty (for experimental control). Note that the pressure drop across the OHP and nozzle/diffuser, for the investigated flow rate of 350 (±20) CFM, was found to be approximately 62 (±3) Pa. This pressure drop value also includes the losses related to the flow in diffuser-duct configuration.

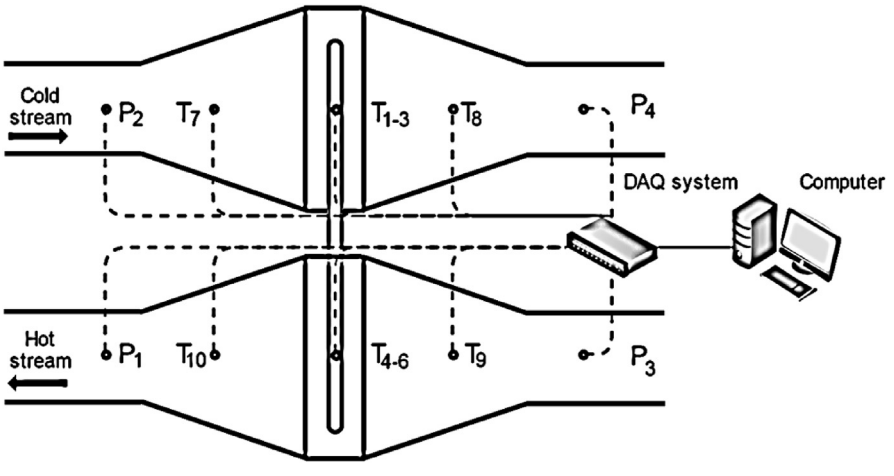

Fig. 4. Approximate locations of thermocouples (Ti) and pressure sensors (Pi) along the center of each air stream within the wind tunnel setup (side view).

https://doi.org/10.1016/j.heliyon.2018.e00922

Table 1. Description of experimental setup.

Material of OHP tube	Copper Alloy 122
Outer diameter of OHP tube	3.18 mm
Inner diameter of OHP tube	1.65 mm
OHP turns	9
Working fluid	n-pentane
Area of OHP evaporator	0.29 m^2 (0.45 × 0.63 m^2)
Area of OHP condenser	0.29 m^2 (0.45 × 0.63 m^2)
Area between evaporator and condenser	0.016 m^2 (0.025 × 0.63 m^2)
Frontal area of OHP in evaporator section	0.14 m^2 (0.30 × 0.46 m^2)
Frontal area of OHP in condenser section	0.14 m^2 (0.30 × 0.46 m^2)
Frontal area of OHP in adiabatic section	0.012 m^2 (0.02 × 0.46 m^2)

4. Calculation

4.1. Uncertainty analysis

The heat transfer through the OHP was approximated using the effectiveness-NTU method [35]. Since the thermal resistance of the OHP evaporator/condenser is much lower than that of the external convection, the OHP was idealized as a device exchanging heat with surroundings via condensation and evaporation of working fluid exclusively (i.e. no sensible heating/cooling of working fluid) [36]. The total heat transfer to the OHP, q_{gain}, from the hot air stream was estimated using Eq. (2):

$$q_{gain} \cong \varepsilon_h q_{max} \tag{2}$$

where the maximum heat transfer rate of the OHP, q_{max}, was found using Eq. (3):

$$q_{max} = C_{min}(T_{hi} - T_{ci}) \tag{3}$$

where T_{hi} is the average temperature of the hot inlet air stream, T_{ci} is the average temperature of the cold inlet air stream, and C_{min} is the minimum heat capacity rate between the hot and cold air streams.

The OHP effectiveness, for either the hot or cold air stream side, was estimated experimentally using Eq. (4). This experimentally-obtained OHP effectiveness, ε_{exp}, was measured when temperature oscillations along the OHP length obtained a steady mean temperature.

$$\varepsilon_{exp} = \frac{q_{exp}}{q_{max}} \cong \frac{\dot{m}_c c_{pc} \Delta T_c}{q_{max}} \tag{4}$$

where $\dot{m}_c$ is the mass flow rate of the cold inlet air stream, c_{pc} is the specific heat of the cold inlet air stream, and ΔT_c is the temperature difference between inlet and outlet of cold air stream.

https://doi.org/10.1016/j.heliyon.2018.e00922

The mean temperatures of the OHP condenser and evaporator were found by taking the arithmetic average of thermocouple measurements in that specific region, as shown by Eqs. (5) and (6), respectively. The effective thermal resistance of the OHP, R, was defined as the quotient between the mean evaporator-to-condenser temperature difference, ΔT_{OHP}, and OHP heat transfer, q_{gain}, as shown in Eq. (7).

$$\overline{T}_{\mathrm{ci,avg}} = \frac{\overline{T}_1 + \overline{T}_2 + \overline{T}_3}{3} \tag{5}$$

$$\overline{T}_{\mathrm{hi,avg}} = \frac{\overline{T}_4 + \overline{T}_5 + \overline{T}_6}{3} \tag{6}$$

$$R = \frac{\overline{T}_{\mathrm{hi,avg}} - \overline{T}_{\mathrm{ci,avg}}}{q_{\mathrm{gain}}} = \frac{\Delta T_{\mathrm{OHP}}}{q_{\mathrm{gain}}} \tag{7}$$

where $\overline{T}_{\mathrm{j}}$ is the time-averaged steady mean temperature of j$^{\mathrm{th}}$ thermocouple (as shown in Fig. 4) and $\overline{T}_{\mathrm{hi,avg}}$ and $\overline{T}_{\mathrm{ci,avg}}$ are the average temperatures of $\overline{T}_{\mathrm{j}}$ for the evaporator and condenser sections, respectively.

All air properties were evaluated at an OHP surface film temperature, T_{f}, as shown in Eq. (8), where $T_{\mathrm{air,i}}$ is the temperature of inlet air, $T_{\mathrm{air,o}}$ is the temperature of outlet air and $\overline{T}_{\mathrm{sc}}$ is the time-averaged, surface temperature of the center-most OHP tube.

$$T_{\mathrm{f}} = \frac{(T_{\mathrm{air,i}} + T_{\mathrm{air,o}})/2 + \overline{T}_{\mathrm{sc}}}{2} \tag{8}$$

Eq. (9) was used to estimate a theoretical waste heat recovery rate of the OHP, q_{th}, i.e.:

$$q_{\mathrm{th}} = \varepsilon_{\mathrm{th}} q_{\mathrm{max}} \tag{9}$$

The investigated OHP represents a unit row of widely spaced (i.e. $S_T/D_{\mathrm{o}} > 3$) 'tubes'; hence, the surface/air heat transfer was assumed similar to flow over a single cylinder in a cross flow [37, 38, 39]. By idealizing the OHP as a row of aligned/parallel cylinders, the mass flow rate ($\dot{m}_{\mathrm{h}}$) and Reynolds number (Re_{h}) of the hot air stream were found using Eqs. (10) and (11), respectively, i.e.:

$$\dot{m}_{\mathrm{h}} = A_{\mathrm{diff}} v_{\mathrm{diff}} \rho_{\mathrm{h}} \tag{10}$$

$$\mathrm{Re}_{\mathrm{h}} = \frac{\rho_{\mathrm{h}} v_{\mathrm{diff}} D_{\mathrm{h}}}{\mu_{\mathrm{h}}} \tag{11}$$

where A_{diff} is the cross-sectional area of the diffuser outlet, v_{diff} is the velocity of air stream at the diffuser outlet, and D_{h} is the hydraulic diameter of the diffuser outlet. The Nusselt number (Nu_{h}) and average heat transfer coefficient ($\overline{h}_{\mathrm{h}}$) were determined using Eqs. (12) and (13), respectively [39].

https://doi.org/10.1016/j.heliyon.2018.e00922

$$\overline{\mathrm{Nu}}_{\mathrm{h}} = \left[0.3 + \left(\frac{0.62\mathrm{Re}_{\mathrm{h}}{}^{1/2}\mathrm{Pr}_{\mathrm{h}}{}^{1/3}}{\left[1+\left(\frac{0.4}{\mathrm{Pr}_{\mathrm{h}}}\right)^{2/3}\right]^{1/4}}\left[1+\frac{\mathrm{Re}_{\mathrm{h}}}{282000}\right]^{5/8}\right)\right]^{4/5} \tag{12}$$

$$\overline{h}_{\mathrm{h}} = \frac{\overline{\mathrm{Nu}}_{\mathrm{h}} k_{\mathrm{h}}}{D_{\mathrm{o}}} \tag{13}$$

where Pr_{h} is the Prandlt number of the hot air stream and k_{h} is the thermal conductivity of the hot air stream.

The number of transfer units ($\mathrm{NTU}_{\mathrm{h}}$), and evaporator-side effectiveness (ε_{h}) were estimated using Eqs. (14) and (15), respectively:

$$\mathrm{NTU}_{\mathrm{h}} \cong \frac{\mathrm{A}_{\mathrm{ohp,h}}\overline{h}_{\mathrm{h}}}{c_{\mathrm{ph}}\dot{m}_{\mathrm{h}}} \tag{14}$$

$$\varepsilon_{\mathrm{h}} \cong 1 - \mathrm{e}^{-\mathrm{NTU}_{\mathrm{h}}} \tag{15}$$

where $A_{\mathrm{ohp,h}}$ is the heat transfer surface area of the OHP in the hot stream and c_{ph} is the specific heat capacity of the hot air stream. The heat transfer from the OHP condenser was calculated using the same procedure outlined by Eqs. (9, 10, 11, 12, 13, 14, 15). Eqs. (16, 17, 18, 19) were used to estimate the overall theoretical effectiveness of the OHP, $\varepsilon_{\mathrm{th}}$, [35, 39], i.e.:

$$C_{\mathrm{c}} \cong \dot{m}_{\mathrm{c}} c_{\mathrm{pc}} \tag{16}$$

$$C_{\mathrm{h}} \cong \dot{m}_{\mathrm{h}} c_{\mathrm{ph}} \tag{17}$$

$$C \cong \frac{\min\left(c_{\mathrm{ph}},\, c_{\mathrm{pc}}\right)}{\max\left(c_{\mathrm{ph}},\, c_{\mathrm{pc}}\right)} \tag{18}$$

$$\varepsilon_{\mathrm{th}} = \left[\frac{1}{\min\left(\varepsilon_{\mathrm{h}},\, \varepsilon_{\mathrm{c}}\right)} + \frac{C}{\max\left(\varepsilon_{\mathrm{h}},\, \varepsilon_{\mathrm{c}}\right)}\right]^{-1} \tag{19}$$

where C_{h} is the heat capacity rate of the hot air stream, c_{pc} is the specific heat capacity of the cold air stream, C_{c} is the heat capacity rate of the cold air stream, $\dot{m}_{\mathrm{h}}$ is the mass flow rate of the hot air stream, $\dot{m}_{\mathrm{c}}$ is the mass flow rate of cold air stream, ε_{h} is the hot air side effectiveness and ε_{c} is cold air side effectiveness.

5. Analysis

The uncertainty related to the measured OHP heat recovery rate was found using linear uncertainty propagation (i.e., the first order Taylor series expansion approximation) [40, 41, 42]. The data reduction equation, relating the heat recovery rate

https://doi.org/10.1016/j.heliyon.2018.e00922

Table 2. Estimated uncertainties for input variables.

Input variables	Estimated uncertainty
Mass flow rate, $\dot{m}_c$	0.007 kg/s
Specific heat, c_{pc}	0 kJ/kg·K
Temperature difference across the OHP in cold air stream, ΔT_c	0.283 °C

(q_{exp}) with measured variables during experimentation, X_i, is shown in Eq. (20) and the uncertainty in q_{exp} was estimated using Eq. (21). Note that mass flow rate of cold air stream, $\dot{m}_c$, and temperature difference in cold air stream across the OHP, ΔT_c, are the measured variables.

$$q_{exp} = \dot{m}_c c_{pc} \Delta T_c \tag{20}$$

$$U_q^2 = \left(\frac{\partial q}{\partial m_c}\right)^2 U_{mc}^2 + \left(\frac{\partial q}{\partial c_{pc}}\right)^2 U_{cp}^2 + \left(\frac{\partial q}{\partial \Delta T}\right)^2 U_{\Delta Tc}^2 \tag{21}$$

In Eq. (21), U_q is the total systematic uncertainty associated with q_{exp} and $\frac{\partial q}{\partial X_i}$ are the absolute sensitivity coefficients of X_i. In this analysis only the systematic type of uncertainty was considered. The systematic uncertainty in estimating q can arise from, for example: (1) air pressure and temperature measurements through sensors, (2) assuming average air specific heat capacities in Eq. (21) and, (3) assuming constant air density in estimating mass flow rate.

The estimation of uncertainties arising from air pressure and temperature measurements involves determination of data acquisition error,[1] spatial temperature non-uniformity error, and calibration error. Uncertainty due to the assumption of average specific heat capacity is negligible in comparison to uncertainty arising from other components. Table 2 shows the estimated uncertainty value for each input variable.

6. Results & discussion

The OHP was found to operate when filled with n-pentane at both fill ratios investigated. This was evidenced by periodic temperature oscillations on its surface during experimentation; indicating internal fluid rearrangement due to the temperature difference imposed by the air streams. The experimentally-measured effectiveness, thermal resistance and heat recovery rate of the OHP for the various investigated fill ratios (FRs) of n-pentane (i.e., 0%, 60% and 70%) are summarized in Table 3.

[1] The data acquisition error is calculated using the guidelines and accuracy of sub-components stated by National Instrument – http://digital.ni.com/public.nsf/allkb/8BA2242D4BCC41B286256D1D00815B90.

https://doi.org/10.1016/j.heliyon.2018.e00922

Table 3. Thermal performance metrics of OHP with various fill ratios of n-pentane.

Thermal performance	FR = 70%	FR = 60%	FR = 0%
OHP-HE effectiveness	0.05	0.04	0.02
Effective thermal resistance (°C/W)	0.11	0.13	0.25
Heat recovery rate (W)	225	170	110

The heat transfer ability of the OHP is confirmed by it outperforming the empty copper tubing (i.e. the empty 'OHP').

As shown in Table 3, the OHP performed optimally while filled n-pentane at FR = 70%. This 'OHP-FR70' demonstrated an average heat recovery rate of 225 W, while possessing an effectiveness of 0.05 and an effective thermal resistance of 0.11 °C/W. Relative to the OHP-FR0 (i.e. the empty OHP), the OHP-FR70 essentially increases total heat transfer between air streams by a factor of 2. The effective thermal resistance of the OHP-FR70 was approximately 60% less than the OHP-FR0 − which was near 0.25 °C/W. The heat transfer ability of the OHP-FR70 was approximately 25% higher than that of the OHP-FR60 (i.e. OHP with FR = 60%). This demonstrates the sensitivity of OHP-HE heat recovery rate on the FR of the OHP. In using OHPs with relatively low FRs, enhanced heat recovery rates are less consistent with time, since the steady-state fluid distribution consists of less liquid present, on average, in the evaporator during operation. Using a FR that is at least greater than the non-heated volume of the OHP will increase the probability of having more consistent OHP operation with fewer vapor pressure balances, and thus more fluidic motion, along the turns. With higher FRs, the probability for liquid volume to prevent/alleviate pressure balancing is generally higher. With excessively-high FRs, i.e. > 0.85, in which the evaporator becomes overloaded with liquid, fluid oscillation within the OHP is reduced [25] and the heat transfer is representative of that found in a capillary-scale thermosyphon. Since it was observed that the n-pentane filled OHP performed better at a FR = 70%, many of the presented results are for this experimental condition only.

Fig. 5 provides a typical temperature response of the OHP-FR70, where T_{in} is the temperature of inlet hot air stream, $\overline{T}_{ci,avg}$ is the average OHP condenser temperature and $\overline{T}_{hi,avg}$ is the average OHP evaporator temperature. Various operating regimes of the OHP were observed and the approximate times in which these regimes transition are labeled. Note that individual temperature responses at various thermocouple locations, along either the condenser or evaporator, demonstrated similar oscillating behavior. As shown in Fig. 5, the OHP-HE temperature field oscillated with respect to time after a critical heat flux was achieved and this indicates its ability to function when using forced convection with air, HVAC-type heating/cooling boundary conditions. The results demonstrate that once the OHP-HE achieves a minimum start-up

https://doi.org/10.1016/j.heliyon.2018.e00922

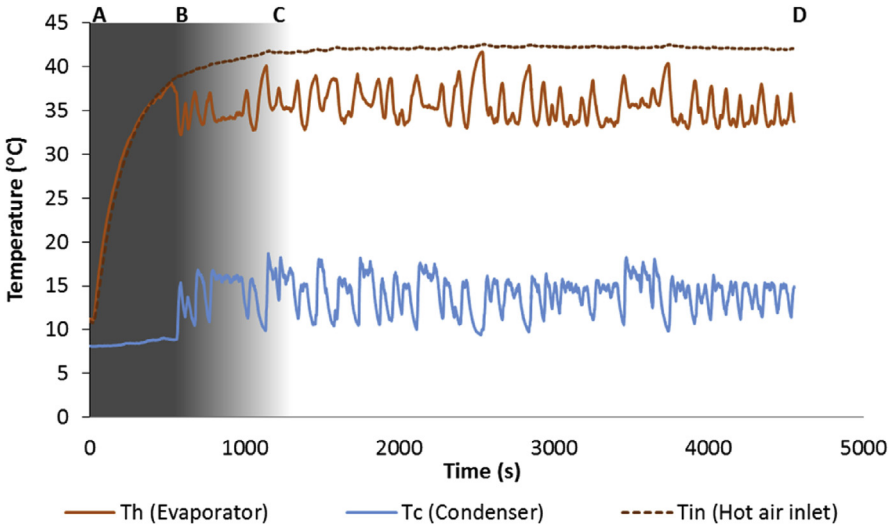

Fig. 5. Averaged temperature response of the OHP-HE with FR = 70% n-pentane with operating regimes AB, BC, and CD indicated via shaded zones.

heat flux, the n-pentane working fluid starts to pulsate at a relatively low frequency and high amplitude – indicating the presence of cyclic evaporation and condensation. The consistent temperature oscillations with respect to time indicate reliable OHP operation. Marked temperature drops in the evaporator were observed to correspond to temperature increases within the condenser. The OHP-HE heat recovery rate from the hot air duct to the cold air duct was found to vary with time, but ranged between 200-250 W.

As shown in Fig. 5, the OHP displayed three different operating regimes during time intervals: AB, BC, and CD. Each of these operating regimes are characterized by distinct temperature oscillations, and thus, internal fluidic behavior [11]. Regime AB corresponds to the time invested for 'pre-heating' the OHP, in which the heat transfer is predominantly conduction along the OHP tube structure and free convection within the entrained working fluid. No temperature oscillations were observed during this time. Point B is the point in time in which the OHP 'awakens' due to the heat flux, and temperature, being conducive for liquid phase-change, and subsequent bubble growth and expansion in the evaporator. The temperature of the evaporator sharply decreases due to the phase change heat transfer, while the temperature of the condenser responds with a temperature increase due to forced convection and condensation heat transfer. Both the BC and CD regimes correspond to time intervals in which the internal fluid is oscillating in regular intervals. For OHPs with typical form factors and operating frequencies (i.e. < 1 Hz), the BC regime is typically characterized by the existence of bubble-type flow while the CD regime corresponds to more slug-type flow pattern conditions [43]. For the current investigation, the BC regime corresponds to a transition period in OHP operation, in which fluid motion is more intermittent and less periodic [43].

https://doi.org/10.1016/j.heliyon.2018.e00922

Table 4. Experimental conditions at start-up of the OHP with FR = 70% n-pentane.

Time elapsed for the OHP-HE to start-up	~500 s
Temperature of hot air stream at start-up	38.2 ± 0.28 °C
Temperature of cold air stream at start-up	8 ± 0.28 °C
Temperature difference across the OHP-HE at start-up	30 ± 0.28 °C

The approximate start-up conditions, as measured for the OHP-FR70 are provided in Table 4. It is important to note, that in addition to the OHP fill ratio, the conditions required for start-up will additionally depend on OHP design (e.g. tube diameter, length, etc.), operating conditions (e.g. OHP orientation, heating/cooling lengths, heating/cooling heat transfer rates), working fluid thermophysical properties (e.g. latent heat of vaporization, specific heat capacity), working fluid rheological properties (e.g. surface tension, viscosity) and the surface roughness of the internal tube structure [10]. Hence, the OHP design and working fluid selection should be carefully considered for ensuring a critical heat flux is achievable for a given HVAC application.

Fig. 6(a) and (b) provides the average, steady-state evaporator/condenser temperature oscillations along the surface of the OHP-FR70 and OHP-FR60, respectively. The temperature oscillations are shown over an arbitrary 1000 s time interval in order to discern oscillation characteristics more easily. From Fig. 6(a) and (b), it may be seen that both OHPs have evaporator and condenser temperatures that oscillate with respect to time. Temperature increases in the evaporator were accompanied with similar-natured temperature decreases in the condenser. Both OHPs have temperature oscillations with characteristic frequencies on-the-order of 10 mHz, which is approximately 2 orders of magnitude lower than those found on OHPs with shorter form factors while undergoing constant heat flux evaporator conditions [44]. This very low frequency operation of the OHP-HE suggests that thin film evaporation, which is a typical mechanism for heat transfer in many OHPs [45, 46], may not be the dominant means for phase change of working fluid in the evaporator. Instead, the time scales inherent to fluid oscillations observed herein suggest that boiling heat transfer is more prominent in the OHP-HE evaporator. Relative to the OHP-FR60, the OHP-FR70 possessed steady-state temperature oscillations typically higher in amplitude and lower in frequency. Due to the higher volume of working fluid inside the OHP-FR70, the time required for the evaporator to 'push' liquid into the condenser is typically higher. The higher amplitude can be attributed to the more latent heat transfer, due to larger fluid volumes, in the evaporator and condenser.

Fig. 7 provides the heat recovery rate (heat transfer from the hot to cold air stream) by the OHP-FR70. The heat transfer is oscillatory due to the cyclic phase-change heat transfer within the OHP. Since sensor noise was evident in the measured

https://doi.org/10.1016/j.heliyon.2018.e00922

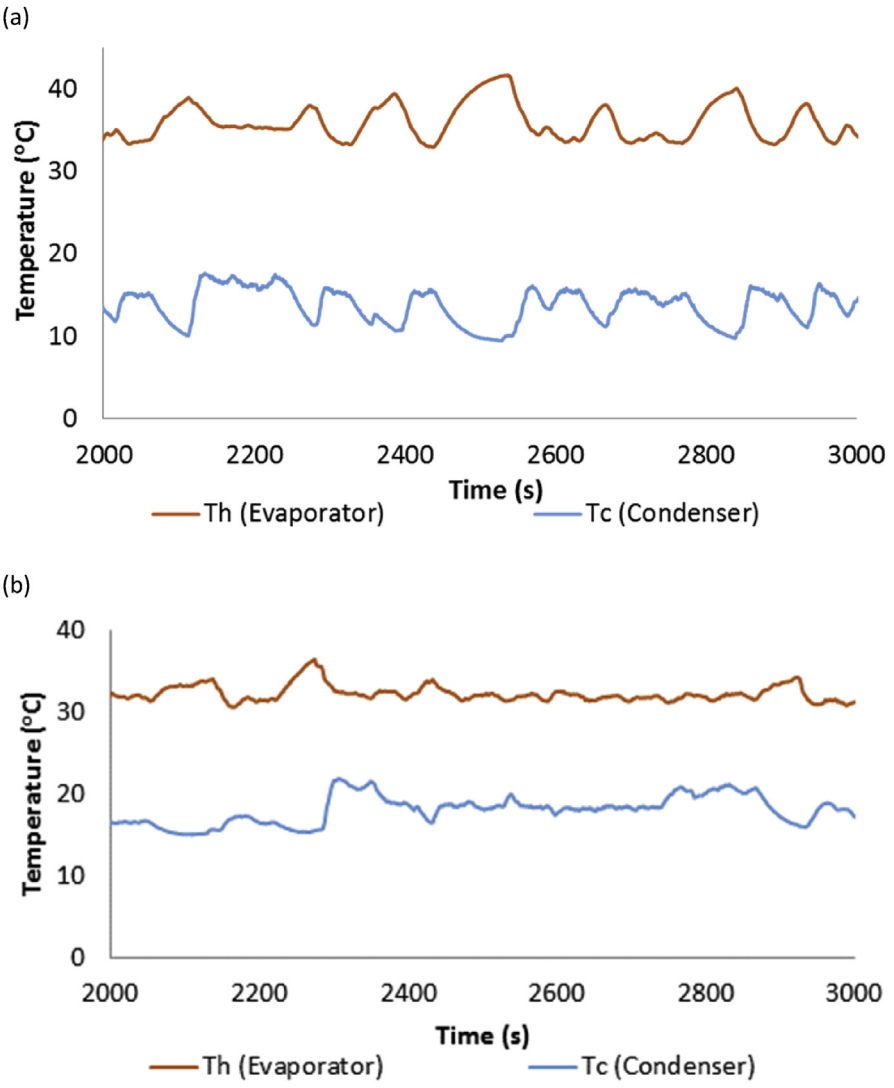

Fig. 6. Steady-state temperature oscillations of evaporator and condenser of the OHP-HE filled with (a) FR = 70% n-pentane and (b) FR = 60 % n-pentane.

oscillatory heat rate, a Savitzky-Golay filter [47], which is a generalized moving average smoothing technique, was applied for data smoothing. This sensor noise was also accounted for during uncertainty quantification. From Fig. 7, it may be seen that the average heat recovery rate was measured to be approximately 225 W, with a peak heat rate of 250 W. Heat transfer between air streams was observed to increase with respect to time until leveling-off at approximately 5000 s, suggesting a 'conditioning' operating regime of the OHP, in which its thermal performance is still adjusting at a longer time scale. This OHP conditioning period may be due to the oscillation of working fluid in OHP-HE decreasing the overall thermal resistance of the copper tube with time. The OHP heat transfer was found to vary with operating regime – being lowest prior to its start-up and highest during the CD regime.

https://doi.org/10.1016/j.heliyon.2018.e00922

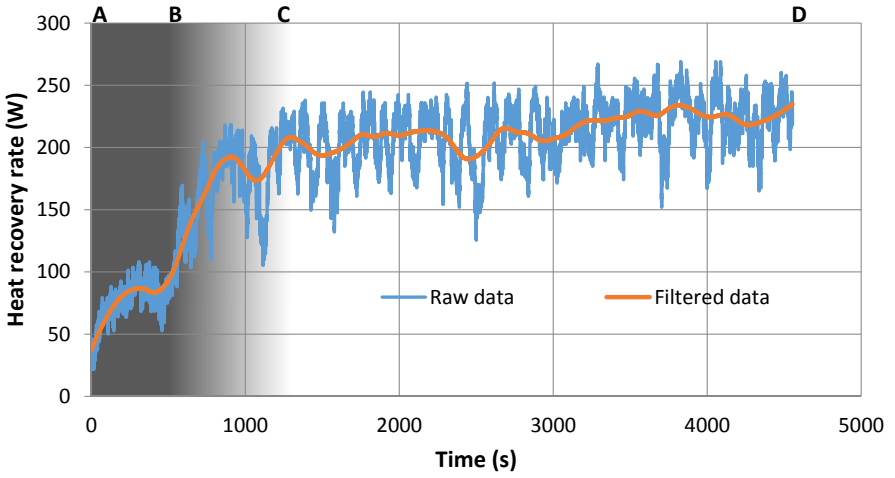

Fig. 7. OHP-HE with FR = 70% n-pentane heat recovery rate vs. time with operating regimes AB, BC, and CD indicated via the shaded zones.

Fig. 8 compares the theoretically-estimated, maximum heat transfer rate with the experimentally-measured heat transfer rate through the OHP-FR70 and OHP-FR0 during steady-state operation. The utility of the OHP-HE over flat plate heat exchangers is demonstrated in that the phase-change heat transfer offered by the oscillating working fluid allows for a significant increase in waste heat recovery. Fig. 8 also demonstrates that the theoretically-estimated, maximum heat transfer rate lies within the range of uncertainty of the experimentally measured heat transfer rate. Hence, the assumptions made for use of the ε-NTU formulation are reasonable and it is confirmed that the internal thermal resistance of the OHP is considerably lower than the external, surface/air thermal resistance.

The unit-row OHP-HE investigated herein consists of a simplistic, non-optimized design. Its ability to function while possessing a long form factor and undergoing forced convection with HVAC-typical air flow was confirmed. Still, the potential energy savings related to employing the OHP-HE in a conventional, commercial-type

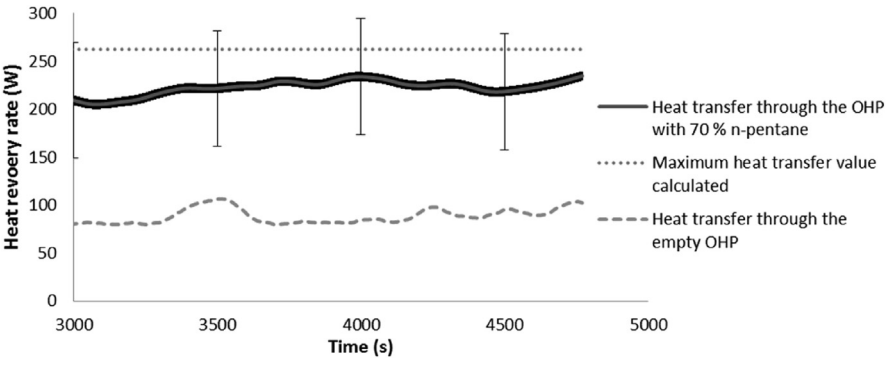

Fig. 8. Comparison of measured, steady-state heat transfer through OHP-FR70 and OHP-FR0 with theoretical, maximum heat transfer.

https://doi.org/10.1016/j.heliyon.2018.e00922

HVAC system can be estimated by using the measured thermal performance of the OHP-FR70. The results suggest that approximately 200 W of power can be saved using only a unit-row OHP-HE for pre-heating/cooling HVAC air. In application, this recovered energy can, for example, increase air inlet temperatures to electric/furnace-based heaters for decreasing their thermal load, resulting in reduced spending on electricity/fuel. The efficiency of such applications would depend on the insulation of the air stream ducting − to ensure captured thermal energy is not transferred to surrounding environment.

The OHP-HE investigated herein possesses a relatively low effectiveness, i.e. 0.04−0.05, when compared to heat pipe heat exchangers already found in the field [48, 49, 50]. However, the investigated OHP-HE was designed only for proof-of-concept experimentation and consists of only a single, un-finned tube. A more optimized OHP-HE design, with higher effectiveness, can be achieved by employing multiple finned OHPs to form an array. In addition, the OHP wetted frontal area, or footprint, was approximately half of the available ducting cross-sectional area. Although this is beneficial for reducing the OHP-HE pressure drop, a significant portion of waste heat was 'un-recovered'. The theoretical effectiveness of the OHP-HE at the evaporator side, ε_h, was found to be 0.12; implying that ~12% of available heat is being gained by the OHP tube structure within the hot stream. Finned surfaces should increase this value.

7. Conclusions

The feasibility in using tubular OHPs within HVAC ducting systems for the task of waste heat recovery has been experimentally investigated. The working fluid, n-pentane, was utilized due to its compliable properties and the OHP fill ratio (FR) was varied between 0%, 60% and 70%. The results show that, even when using a relatively simple OHP design (un-finned and unit row), up to 240 W of heat can be recovered from an air stream in typical HVAC operating conditions. The OHP heat exchanger (OHP-HE) demonstrates to be relatively aerodynamic − providing a pressure drop of <60 Pa while positioned in both air streams. Among all fill ratios tested, The OHP with n-pentane at FR = 70% provided for maximum heat transfer, which was found to be almost twice that accomplishable via the empty OHP. Distinct operating regimes of the OHP were observed during its transient response, as evidenced by different surface temperature oscillation patterns occurring with respect to time. The results demonstrate that the OHP is fully-capable of operating in the air-to-air convection mode for waste heat recovery for typical HVAC operating conditions. In addition, the relatively long form factor OHP has been found operable; however, its operation may be more prone to boiling heat transfer in the evaporator, as well as temperature oscillations with very low frequencies, on-the-order of 10 mHz.

https://doi.org/10.1016/j.heliyon.2018.e00922

The demonstrated OHP-based heat recovery system is advantageous in that it works passively without any additional energy input and possesses a minimal pressure drop. The OHP is relatively simple to manufacture since it consists of no internal wicking structure. The OHP-HE can be installed between segregated HVAC ducts with streams of unlike temperature; where unmixed ventilation heat recovery is desirable in buildings and industrial facilities such as hospitals, recreation centers and more. More sophisticated OHP-HEs, with optimized configurations (e.g. fins, more rows) and different working fluids, would most likely increase heat recovery rates.

Declarations

Author contribution statement

Govinda Mahajan: Conceived and designed the experiments; Performed the experiments; Analyzed and interpreted the data; Wrote the paper.

Scott M. Thompson: Conceived and designed the experiments; Analyzed and interpreted the data; Contributed reagents, materials, analysis tools or data; Wrote the paper.

Heejin Cho: Conceived and designed the experiments; Analyzed and interpreted the data; Wrote the paper.

Funding statement

This work was supported by the National Science Foundation (CBET-1403872), the Bagley College of Engineering and the Department of Mechanical Engineering at Mississippi State University (MSU).

Competing interest statement

The authors declare no conflict of interest.

Additional information

No additional information is available for this paper.

References

[1] Transition to Sustainable Buildings: Strategies and Opportunities to 2050, 2013.

[2] L. Pérez-Lombard, J. Ortiz, C. Pout, A review on buildings energy consumption information, Energy Build. 40 (2008) 394–398.

https://doi.org/10.1016/j.heliyon.2018.e00922

[3] K.W. Roth, D. Westphalan, J. Dieckmann, S.D. Hamilton, W. Goetzler, Energy Consumption Characteristics of Commercial Building HVAC Systems Volume III, Energy savings potential, Cambridge, MA, 2002.

[4] ASHRAE, ASHRAE Handbook- HVAC Systems and Equipment, Atlanta, GA, 2012.

[5] M.A. Abd El-Baky, M.M. Mohamed, Heat Pipe heat exchanger for heat recovery in air conditioning, Appl. Therm. Eng. 27 (2007) 795−801.

[6] G.P. Peterson, An Introduction to Heat Pipes. Modeling, Testing, and Applications, first ed., Wiley, New York, Chichester, 1994.

[7] G.M. Grover, T.P. Cotter, G.F. Erickson, Structures of very high thermal conductance, J. Appl. Phys. 35 (1964) 1990−1991.

[8] T. Xin, S. Lili, Z. Hua, J. Yonglin, A review of recent experimental investigation and theoretical analysis for pulsating heat pipe, Front. Energy 7 (2013) 161−173.

[9] S. Khandekar, M. Groll, An insight into thermo-hydrodynamic coupling in closed loop pulsating heat pipes, Int. J. Therm. Sci. 43 (2004) 13−20.

[10] W. Qu, H.B. Ma, Theoretical analysis of startup of a pulsating heat pipe, Int. J. Heat Mass Tran. 50 (2007) 2309−2316.

[11] S. Khandekar, N. Dollinger, M. Groll, Understanding operational regimes of closed loop pulsating heat pipes: an experimental study, Appl. Therm. Eng. 23 (2003) 707−719.

[12] S.M. Thompson, B.S. Tessler, H.B. Ma, D.E. Smith, A. Sobel, Ultra-high thermal conductivity of three-dimensional flat-plate oscillating heat pipes for electromagnetic launcher cooling. Proc. IEEE 2012 16th Int. Symp. Electromagn, Launch Technol., Beiging, China, 2012.

[13] Y.-H. Lin, S.-W. Kang, H.-L. Chen, Effect of silver nano-fluid on pulsating heat pipe thermal performance, Appl. Therm. Eng. 28 (2008) 1312−1317.

[14] P. Meena, S. Rittidech, Closed-loop oscillating heat-pipe with check valves (CLOHP/CVs) air-preheater for reducing relative humidity in drying systems, Appl. Energy 84 (2006) 363−373.

[15] D. Yuan, W. Qu, T. Ma, Flow and heat transfer of liquid plug and neighboring vapor slugs in a pulsating heat pipe, Int. J. Heat Mass Tran. 53 (2010) 1260−1268.

[16] W. Qu, Y. Li, T. Ma, Frequency analysis of pulsating heat pipe, in: Proc. ASME InterPACK Conf. Br. Columbia, Vancouver, Canada, ASME InterPack Conference, British Columbia, Vancouver, Canada, 2007, pp. 689−693.

https://doi.org/10.1016/j.heliyon.2018.e00922

[17] N. Bhuwakietkumjohn, S. Rittidech, Internal flow patterns on heat transfer characteristics of a closed-loop oscillating heat-pipe with check valves using ethanol and a silver nano-ethanol mixture, Exp. Therm. Fluid Sci. 34 (2010) 1000−1007.

[18] P. Charoensawan, P. Terdtoon, Thermal performance correlation of horizontal closed-loop oscillating heat pipes, Proc. Electron. Packag. Technol. Conf. EPTC. 28 (2007) 906−909.

[19] T. Katpradit, T. Wongratanaphisan, P. Terdtoon, S. Ritthidech, P. Chareonsawan, S. Waowaew, Effect of aspect ratios and bond number on internal flow patterns of closed end oscillating heat pipe at critical state, in: Proc. 13th Int. Heat Pipe Conf., 2004, pp. 7−80144.

[20] Y. Zhang, A. Faghri, Advances and unsolved issues in pulsating heat pipes, Heat Tran. Eng. 29 (2008) 20−44.

[21] S. Khandekar, M. Groll, Roadmap to realistic modeling of closed loop pulsating heat pipes, in: 9th Int. Heat Pipe Symp. Kuala Lumper, Malaysia, 2008.

[22] P. Cheng, H. Ma, A mathematical model of an oscillating heat pipe, Heat Tran. Eng. 32 (2011) 1037−1046.

[23] P. Supirattanakul, S. Rittidech, B. Bubphachot, Application of a closed-loop oscillating heat pipe with check valves (CLOHP/CV) on performance enhancement in air conditioning system, Energy Build. 43 (2011) 1531−1535.

[24] M. Groll, S. Khandekar, Pulsating heat pipe: progress and prospects, in: Int. Conf. Energy Environ. Shanghai, China, 2003, pp. 20−44.

[25] H.B. Ma, B. Borgmeyer, P. Cheng, Y. Zhang, Heat transport capability in an oscillating heat pipe, J. Heat Tran. 130 (2008), 081501-081501-7.

[26] S.M. Thompson, A.A. Hathaway, C.D. Smoot, C.A. Wilson, H.B. Ma, R.M. Young, L. Greenberg, B.R. Osick, S. Van Campen, B.C. Morgan, D. Sharar, N. Jankowski, Robust thermal performance of a flat-plate oscillating heat pipe during high-gravity loading, J. Heat Tran. 133 (2011) 104504.

[27] S. Khandekar, A. Gupta, Embedded pulsating heat pipe radiators, in: 14th Int. Heat Pipe Conf. Florianopolis, Brazil, 2007, pp. 4−9.

[28] S. Rittidech, W. Dangeton, S. Soponronnarit, Closed-ended oscillating heat-pipe (CEOHP) air-preheater for energy thrift in a dryer, Appl. Energy 81 (2005) 198−208.

https://doi.org/10.1016/j.heliyon.2018.e00922

[29] M. Dilawar, A. Pattamatta, A parametric study of oscillatory two-phase flows in a single turn Pulsating Heat Pipe using a non-isothermal vapor model, Appl. Therm. Eng. 51 (2013) 1328−1338.

[30] G. Burban, V. Ayel, A. Alexandre, P. Lagonotte, Y. Bertin, C. Romestant, Experimental investigation of a pulsating heat pipe for hybrid vehicle applications, Appl. Therm. Eng. 50 (2013) 94−103.

[31] P. Charoensawan, P. Terdtoon, Thermal performance of horizontal closed-loop oscillating heat pipes, Appl. Therm. Eng. 28 (2008) 460−466.

[32] H. Ma, Oscillating Heat Pipes, first ed., Springer-Verlag, New York, 2015.

[33] R. McKee, E. Frank, J. Heath, D. Owen, R. Przygoda, G. Trimmer, F. Whitman, Toxicology of n-pentane (CAS no. 109−66−0), J. Appl. Toxicol. 18 (1998) 431−442.

[34] Pollution Prevention and Abatement Handbook, 1998, World Bank Group, 1999.

[35] W.M. Kays, A.L. London, Compact Heat Exchanger, second ed., McGraw-Hill Book Co, New York, 1964.

[36] S. Khandekar, Pulsating heat pipe based heat exchangers, in: Proc. 21st Int. Symp. Transp. Phenom., 2010, pp. 2−5.

[37] F.P. Incropera, Fundamentals of Heat and Mass Transfer, John Wiley & Sons Australia, Limited, 1992.

[38] S.Y. Yoo, H.K. Kwon, J.H. Kim, A study on heat transfer characteristics for staggered tube banks in cross-flow, J. Mech. Sci. Technol. 21 (2007) 505−512.

[39] S.W. Churchill, M. Bernstein, A correlating equation for forced convection from gases and liquids to a circular cylinder in crossflow, ASME Trans. Ser. C-J. Heat Transf. 99 (1977) 300−306.

[40] H.W. Coleman, W.G. Steele, Experimentation and Uncertainty Analysis for Engineers, second ed., John Wiley & Sons, Inc., 1999.

[41] H. Cho, N. Fumo, Uncertainty analysis for dimensioning solar photovoltaic arrays, in: 6th Int. Conf. Energy Sustain. 10th Fuel Cell Sci. Eng. Technol. Conf. San Diego, CA, San Diego, CA, 2012, pp. 1−5.

[42] ISO, International Organization for Standardization (ISO), Guide to the Expression of Uncertainty in Measurement (Corrected and Reprinted 1995), 1993. Geneva, Switzerland.

https://doi.org/10.1016/j.heliyon.2018.e00922

[43] S. Khandekar, Groll Manfred, On the defination of pulsating heat pipes: an overview, in: 5th Minsk Int. Semin. Pipes, Heat Pumps Refrig. Minsk. Belarus, Minsk, Belarus, 2003.

[44] J.D. Fairley, S.M. Thompson, D. Anderson, Time−frequency analysis of flat-plate oscillating heat pipes, Int. J. Therm. Sci. 91 (2015) 113−124.

[45] G. Spinato, N. Borhani, J.R. Thome, Operational regimes in a closed loop pulsating heat pipe, Int. J. Therm. Sci. 102 (2016) 78−88.

[46] S. Lips, A. Bensalem, Y. Bertin, V. Ayel, C. Romestant, J. Bonjour, Experimental evidences of distinct heat transfer regimes in pulsating heat pipes (PHP), Appl. Therm. Eng. 30 (2010) 900−907.

[47] R.W. Schafer, What is a Savitzky-Golay filter? [Lecture notes], Signal Process. Mag. IEEE. 28 (2011) 111−117.

[48] H. Jouhara, R. Meskimmon, Experimental investigation of wraparound loop heat pipe heat exchanger used in energy efficient air handling units, Energy 35 (2010) 4592−4599.

[49] D. Liu, G.-F. Tang, F.-Y. Zhao, H.-Q. Wang, Modeling and experimental investigation of looped separate heat pipe as waste heat recovery facility, Appl. Therm. Eng. 26 (2006) 2433−2441.

[50] Y.H. Yau, A.S. Tucker, The performance study of a wet six-row heat-pipe heat exchanger operating in tropical buildings, Int. J. Energy Res. 27 (2003) 187−202.

https://doi.org/10.1016/j.heliyon.2018.e00922